

## Electrochemical Noise Analysis on the Effect of Magnetic Field on the Corrosion Susceptibility of Pure Magnesium

Song Wang<sup>1</sup>, Zhongyi Wang<sup>1</sup>, Jian Li<sup>2</sup>, Tao Zhang<sup>2,3,\*</sup>

<sup>1</sup>College of Power and Energy Engineering, Harbin Engineering University, Nantong ST 145, Harbin, 150001, China

<sup>2</sup>Corrosion and protection Laboratory, Key Laboratory of Superlight Materials and Surface Technology (Harbin Engineering University), Ministry of Education, Nantong ST 145, Harbin, 150001, China

<sup>3</sup>Laboratory for Corrosion and Protection, Institute of Metal Research, Chinese Academy of Sciences, Wencui RD 62, Shenyang, 110016, China)

\*E-mail: [zhangtao@hrbeu.edu.cn](mailto:zhangtao@hrbeu.edu.cn)

*Received:* 3 October 2015 / *Accepted:* 11 December 2015 / *Published:* 1 January 2016

---

The effect of magnetic field (MF) on the corrosion susceptibility of pure magnesium was investigated by electrochemical measurements and SEM observation. In the presence of MF, the corrosion process of magnesium showed two distinguishing stages, and MF played contrary roles on the corrosion susceptibility during two stages. During the passivation stage, pure magnesium in the presence of MF showed a passive behavior, which ascribed to the acceleration of oxygen diffusion due to magnetohydrodynamic (MHD) effect. During the pitting corrosion stage, both the pitting initiation rate and pitting growth probability were accelerated by MF, which indicated the significant increase of corrosion susceptibility.

---

**Keywords:** magnesium; electrochemical noise; polarization; stochastic analysis; pitting corrosion

### 1. INTRODUCTION

Among light metals magnesium presents very interesting engineering properties owing to its high specific rigidity, high thermal conductivity and easy recycling. These properties make magnesium very attractive for applications in many industry fields. These potential advantages are diminished by the poor corrosion resistance of Mg and its alloys, due to the high chemical reactivity of magnesium in presence of humidity or solution. In the field of 3C industry (Computer, Communication and Consumer Electronic), magnesium alloys are used as structural materials mostly in electric-magnetic

field environments; however, the literature about magnetic effect on the corrosion of magnesium alloys is scarce.

Magnetic field has a strong influence on the corrosion behavior of metals [1-16]. Magnetic fields affect magnetic species according to their nature (ferromagnetic, paramagnetic or diamagnetic). Electrochemical reactions involving such species will also be affected by the applied magnetic field. Moreover, elementary physics shows that charged particles in motion, such as ions, will be subject to the Lorentz force caused by the application of a magnetic field. Magnetohydrodynamic (MHD) theory is generally used to formulate the effect of magnetic fields on mass transport rates [9-14]. However, the exact influence of magnetic fields on corrosion processes is not well understood, and contradictory results have been reported. General corrosion of an iron plate in 0.5 M sodium chloride was found to be accelerated by an 8 T magnetic field parallel to the plate [15]. On the other hand, general corrosion of copper was found to be suppressed by magnetic fields, while its localized corrosion was found to be accelerated [16]. Magnetic fields have been reported to reduce the corrosion susceptibility of aluminum [17] and 303 stainless steel [18], but the repassivation potential of stainless steel was decreased when a 0.27 T magnetic field was applied perpendicular to the surface [19].

In our previous work, the influence of magnetic field on the corrosion resistance of passivated magnesium was investigated [20], but the detail influence mechanism of magnetic field on the corrosion process of pure magnesium was still not clear. Therefore, in this work, the emphasis was put on it by means of electrochemical noise (EN). The EN result was quantitatively analyzed based on stochastic description of pitting corrosion, taking into account pitting initiation and pitting growth.

## 2. EXPERIMENTAL METHOD

### 2.1 Materials

The specimen for this work was commercial pure magnesium with the purity of 99.99%. All of the specimens were wet ground to a 1000-grit finish, degreased with acetone, rinsed with distilled water and dried in a compressed hot air flow.

The test solution was a mixture of 0.05 M sodium chloride and 0.01 M sodium hydroxide prepared by mixing analysis grade chemicals and distilled water. The pH of the solution was 12.0.

### 2.2 Electrochemical measurement

When experiments were carried out in the presence of MF, The working electrode surface was placed vertically, and the direction of MF was horizontal and parallel to the surface of the working electrode. The magnetic field with magnetic flux density of 0.3 T was generated by a permanent magnet with Nd-Fe-B magnets.

For the measurements of the polarization curves, a conventional three-electrode cell was used, with a standard Ag-AgCl/KCl-sat electrode being used as a reference electrode and a platinum counter

electrode (20 mm×20 mm). The anodic polarization curves were scanned with a scanning rate of 0.333 mV/s from open circuit potential (OCP) towards anodic direction.

For deaerated experiments, the medium was deaerated with nitrogen for 0.5 h before introducing the working electrode. When the experiments went on, a nitrogen atmosphere was maintained above the solution during the experiments to ensure the separation of oxygen.

For the measurements of electrochemical noise, the experiments were performed within a Faraday cage with an AutoLab electrochemical workstation (AutoLab PGSTAT302 produced by Eco Chemie Company) equipped with an electrochemical noise (EN) module. Two identical specimens were used as the working electrode and an Ag-AgCl/KCl-sat electrode was the reference electrode. The electrochemical current noise was the measured galvanic coupling current between two identical working electrodes (WE) kept at the same potential. EN data was simultaneously recorded for 15 h. Each set of EN records was recorded with a data-sampling interval of 0.08 s containing 4096 data points. The DC trend of EN data was removed according to modified-MAR method [21].

For the better reproducibility, all the electrochemical experiments were repeated more than 5 times.

### 2.3 Microstructure observation

The corrosion morphology was observed after the removal of corrosion products. The specimens were immersed in a chromate (200 g/L CrO<sub>3</sub> + 10g/L AgNO<sub>3</sub>) solution for 5 min to remove the corrosion products [22]. Finally, the specimens were washed with deionized water and then dried by hot air flow. The corrosion morphology of pure magnesium in the presence and absence of MF was observed by scanning electronic microscopy (CAMBRIDGE STEREOSCAN 240).

## 3. THEORETICAL BACKGROUND

### 3.1. Shot-noise theory

Shot-noise theory is based on the assumption that the signals are composed of packets of data departing from a base line. This theory can be applied to the analysis of electrochemical noise data from corrosion systems, the current noise signals being considered as packets of charge. Among noise-generating processes, shot-noise is caused by the fact that the current is carried by discrete charge carriers. Consequently, the number of charge carriers passing a given point will be a random variable. Provided that the individual events are independent of other events like the stochastic processes, it has been known that the shot-noise analysis is applicable to the individual events [23-25]. If we assume that shot noise is produced during breakdown of the passive film, pitting initiation and hydrogen evolution, the average corrosion current  $I_{corr}$  is defined as

$$I_{corr} = q \times f_n \quad (1)$$

where  $q$  is the average charge in each event and  $f_n$  the frequency of events.  $f_n$  can be estimated from the following relations based upon the shot-noise theory:

$$f_n = \frac{I_{corr}}{q} = \frac{B^2}{\Psi_E} \quad (2)$$

where  $B$  is the Stern-Geary constant and  $\Psi_E$  is the low frequency limit (0.01 Hz) of power spectral density of potential, respectively.

### 3.2. Stochastic model for pitting initiation

Pitting initiation is modeled using a nonhomogeneous Poisson process [26]. In this way, the distribution of pitting nucleation times can be simulated using the Weibull distributions. The cumulative probability  $F(f_n)$  at each  $f_n$  is numerically determined from the set of  $f_n$  data previously calculated by using Eq. (3). The procedure for determining the cumulative probability  $F(f_n)$  from  $f_n$  data is described as follows: first, all calculated  $f_n$  data are arranged in order from the smallest and then, the cumulative probability  $F(f_n)$  is calculated as  $M/(N + 1)$ , where  $M$  is the rank in the ordered  $f_n$  data and  $N$  the total number of  $f_n$  data. Weibull distribution function is one of the most widely used cumulative probability functions for predicting life time in reliability test [27]. This is because it can easily approximate the normal distribution, logarithmic normal distribution and exponential distribution functions. In addition, it is also possible to analyze data even when two or more failure modes are present at the same time. The cumulative probability  $F(t)$  of a failure system can be introduced just as Weibull distribution function based upon a “weakest-link” model [28-29], which is expressed by Eq. 3

$$F(t) = 1 - \exp\left(-\frac{t^m}{n}\right) \quad (3)$$

where  $m$  and  $n$  are the shape and scale parameters, respectively.  $m$  is a dimensionless parameter and  $n$  is expressed in  $s_m$ . From rearrangement of Eq. (4):

$$\ln\left\{\ln\left[\frac{1}{1-F(t)}\right]\right\} = m \ln t - \ln n \quad (4)$$

By fitting Eq. (5) to the cumulative probability numerically calculated, two parameters  $m$  and  $n$  can be determined from the slope of the linear  $\ln\{\ln[1/(1-F(t))]\}$  versus  $\ln t$  plots and from the intercept on the  $\ln\{\ln[1/(1-F(t))]\}$  axis, respectively.

The conditional event initiation rate  $r(t)$  is employed as a kind of failure rate in reliability engineering, which is defined as

$$r(t) = \frac{m}{n} t^{m-1} \quad (5)$$

Based upon Weibull distribution function, the value of  $r(t)dt$  represents the initiation probability of events in the next unit time  $dt$  for the specimens in which events have not been yet generated when  $t$  has elapsed. This just corresponds to the pitting embryo formation rate in pitting corrosion [27-29].

### 3.3. Stochastic model for pitting depth growth

Pitting depth growth is modeled using a nonhomogeneous Markov process [26]. The way to link the initiation and growth stages when multiple pits are considered is proposed for the first time. To do this, the theoretical foundations of extreme value statistics have been employed. It is shown that the solution of the Kolmogorov forward equations, governing the growth of an individual pit, is in the domain of attraction of the Gumbel distribution [30-34]. The Gumbel extreme value distribution is used to model the deepest pits behavior. The extreme value statistics analysis according to the following procedure: first, all calculated extreme value data are arranged in order from the smallest and then, the probability  $F(Y)$  is calculated as  $1-[M/(N + 1)]$ , where  $M$  is the rank in the ordered extreme value and  $N$  the total number of extreme value data. The reduced variant ( $Y$ ) can be calculated by the formula  $Y = -\ln\{-\ln[F(Y)]\}$  [30-34].

The probability that the largest value of pit depth is described by a double exponent (Gumbel Type extreme value distribution) is expressed in the form [33]:

$$Pit_{max} = \mu + \alpha \ln S \tag{6}$$

$$P = 1 - \exp\left\{-\exp\left[\frac{-(R_{pit} - [\mu + \alpha \ln S])}{\alpha}\right]\right\} \tag{7}$$

Where  $P$  is the probability of pitting size,  $R_{pit}$  is the radius of pit cavity,  $\mu$  is the central parameter (the most frequent value) and  $\alpha$  is the scale parameter, which defines the width of the distribution. In many applications, the Gumbel Type distribution has been claimed to account for the statistical nature in the observed behavior of corrosion systems [26, 31-34]. Specifically, the Gumbel Type extreme value distribution is used for extrapolating corrosion damage measured on a series of small samples of area,  $s$ , to a large system (for example, tanks or pipe lines) with area,  $S$ .

## 4. RESULTS

### 4.1 The electrochemical noise

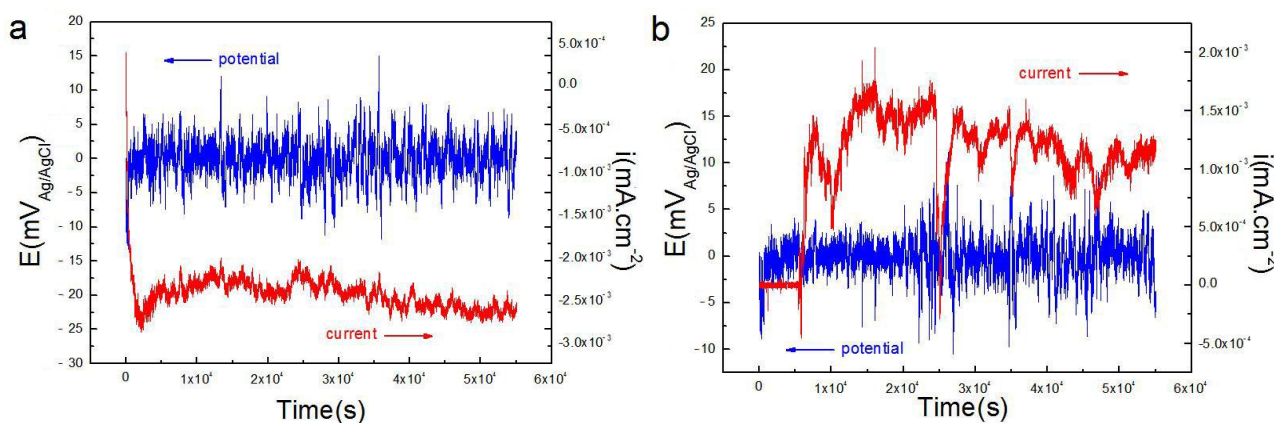
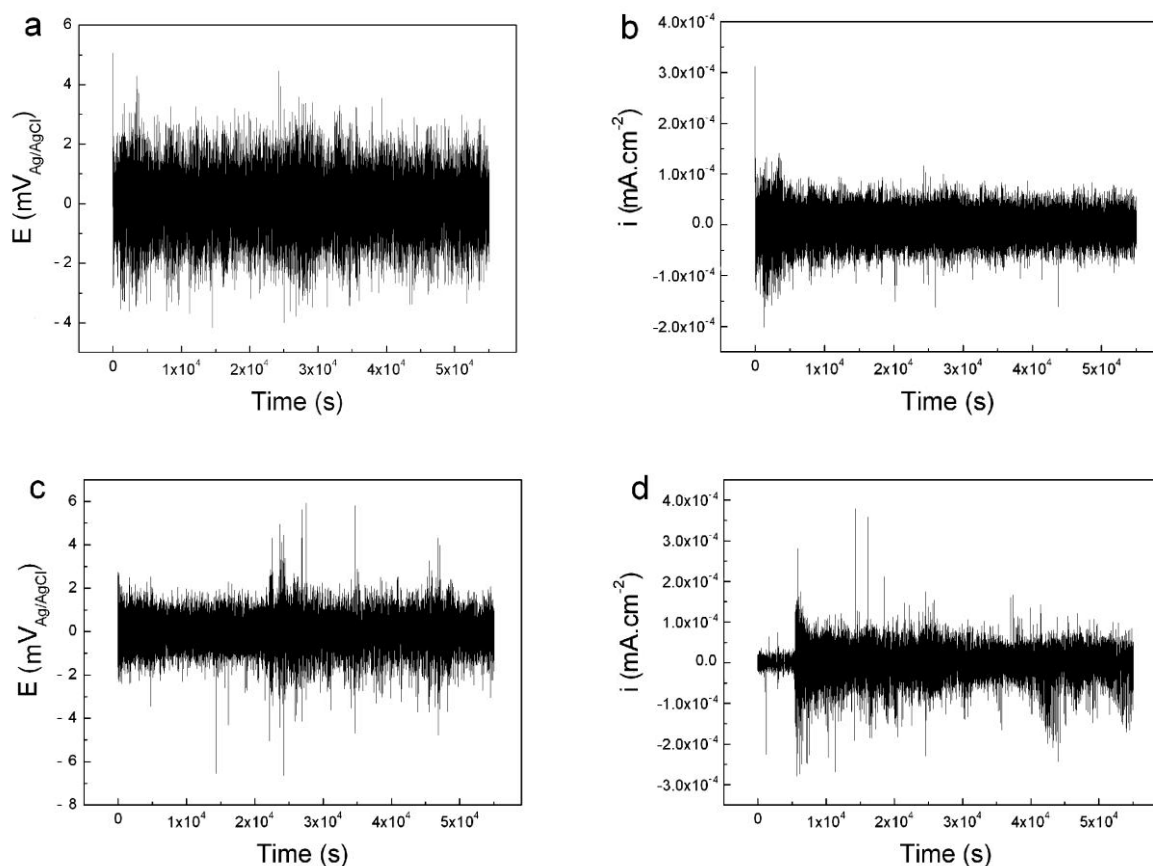


Figure 1. S. Wang et.al. Submitted to Int. J. Electrochem. Sci.

The raw electrochemical noise data for pure magnesium in the absence and presence of MF were shown in Fig. 1 a and b. The potential noise in both experiments showed little variation, but the current noise exhibited strong amplitude fluctuation in the presence of MF. The DC trend of EN data was removed according to modified-MAR method [21] and showed in Fig. 2. After DC trend removal the EN data was analyzed.



**Figure 2.** S. Wang *et.al.* Submitted to *Int. J. Electrochem. Sci.*

#### 4.2 Polarization curves

Polarization curves of pure magnesium after various immersion times (10 min, 3h and 14h) were shown in Fig. 3. Fig. 3 a showed clearly that, in the beginning of the immersion period, the corrosion resistance was strongly improved by MF. The anodic polarization curve in the presence of MF presented a passive behavior while that in the absence of MF presented an active dissolution behavior, which implied the presence of MF evoked the passivation of the specimen. With the increase of the immersion time, and after point A, the corrosion resistance of pure magnesium in case of MF was significantly deteriorated, characterized by the disappear of passive region and the decrease of corrosion potential, which indicated that the anodic electrochemical reaction was promoted by MF (Fig. 3 b, c).

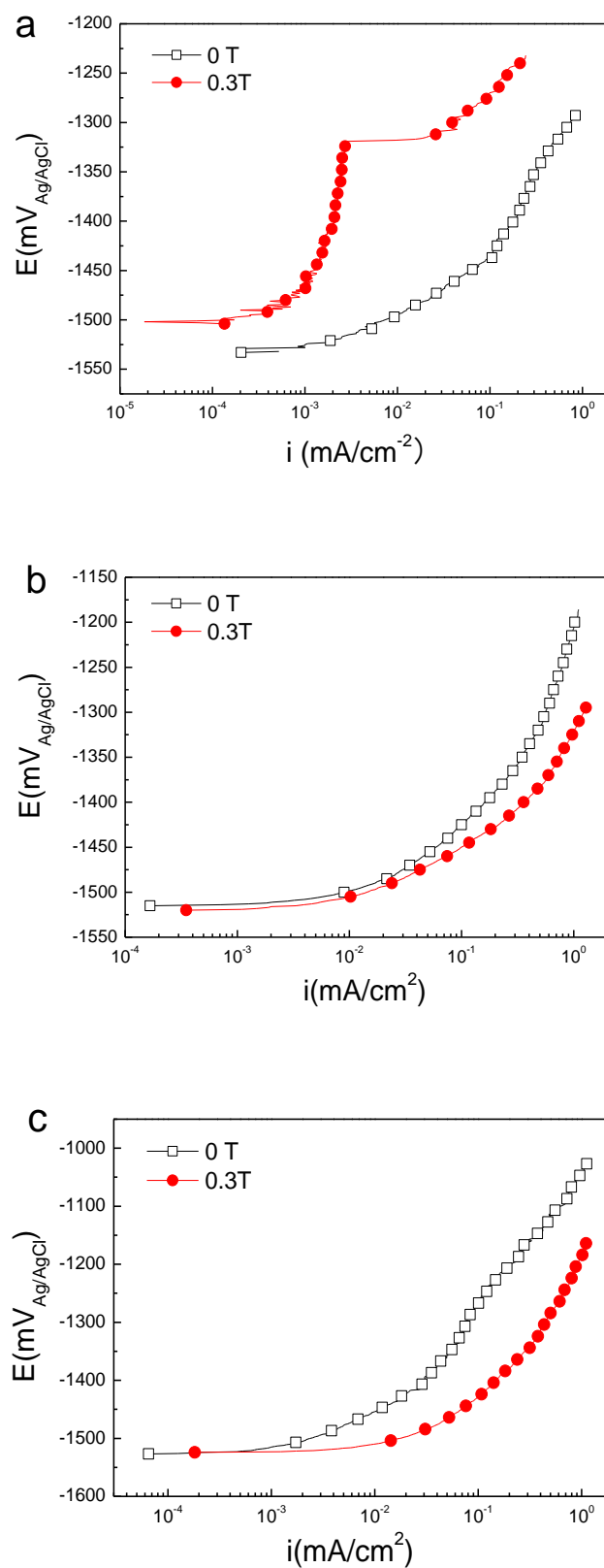
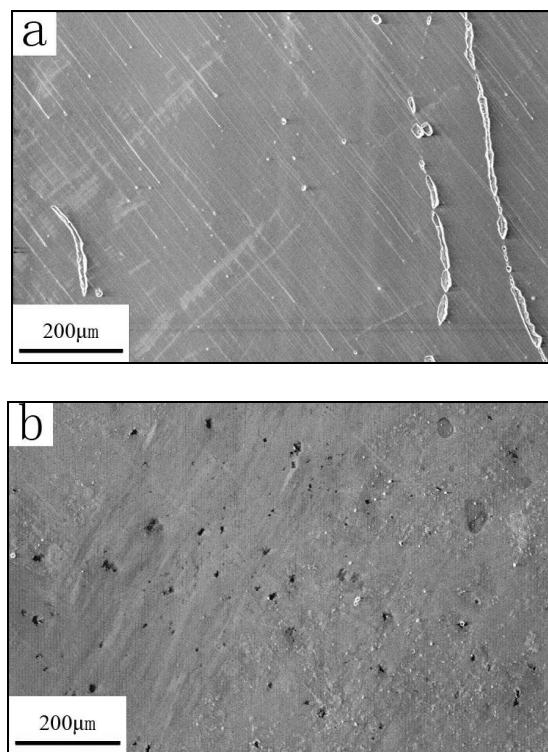


Figure 3. S. Wang et.al. Submitted to Int. J. Electrochem. Sci.

### 4.3 The corrosion morphology observation

The corrosion morphology was observed by scanning electron microscopy (SEM) both before and after point **A** at which the sudden change emerged in the current noise signal.

#### 4.3.1 Corrosion morphology observation after the immersion of 1h



**Figure 4.** S. Wang *et.al.* Submitted to *Int. J. Electrochem. Sci.*

The corrosion morphologies of pure magnesium after the immersion of 1 h (before point **A**) were shown in Fig. 4. Except pitting corrosion, a kind of confused corrosion morphology was observed in the absence of MF (Fig. 4a). There were some arguments on this corrosion morphology. Some researchers suggested crystallographic pitting morphology [35-37]; the others indicated filiform corrosion [38]. In our opinion, filiform corrosion usually underwent beneath the organic coating. Thus, this corrosion morphology should be crystallographic pitting. In the presence of MF, only a little small pitting cavity was observed, Fig. 4 b. The result indicated that at the beginning of the immersion, the pure magnesium in the presence of MF exhibited lower corrosion susceptibility.

#### 4.3.2 Corrosion morphology observation after the immersion of 4.5 h

The corrosion morphologies of pure magnesium after the immersion of 4.5 h (after point **A**) were shown in Fig. 5. After the immersion of 4.5 h, both pitting corrosion and crystallographic pitting were observed in all of the specimens. In the presence of MF, magnesium undertook more serious corrosion. Both the crystallographic corrosion [35-37] and the pitting corrosion could be observed all

over the surface, and the cavity was in a bigger dimension. The results indicated that the presence of MF increased the susceptibility to the pitting corrosion and crystallographic corrosion of pure magnesium.

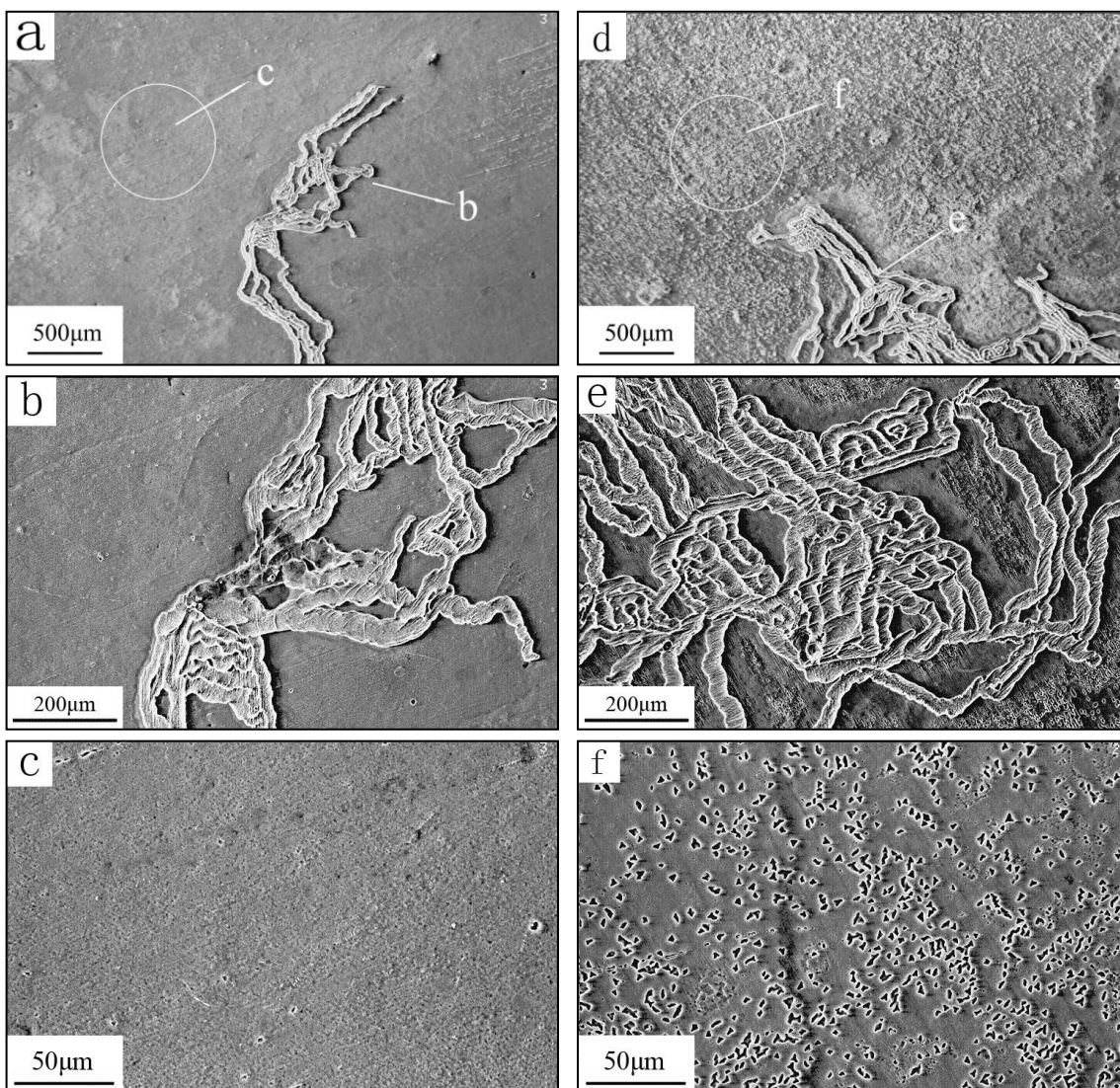


**Figure 5.** *S. Wang et.al. Submitted to Int. J. Electrochem. Sci.*

## 5. DISCUSSION

### 5.1 Effect of magnetic field on the development of corrosion rate

EN data analysis in the time domain involves the calculation of the noise resistance  $R_n$ . Fig. 6 showed the reciprocal of  $R_n$  that was proportional to the corrosion rate which was calculated instantaneously [39, 40]. In the presence of MF, the corrosion rate of magnesium apparently showed two distinguishing stages. In the first stage, the corrosion rate remained a very low level, even lower than that in the absence of MF. In the second stage, the average corrosion rate turned out much higher.  $R_n$  results implied that, in the beginning of the immersion period, the presence of MF decreased the

corrosion rate which indicated pure magnesium was passivated; and after point **A**, it could significantly accelerate the corrosion rate.

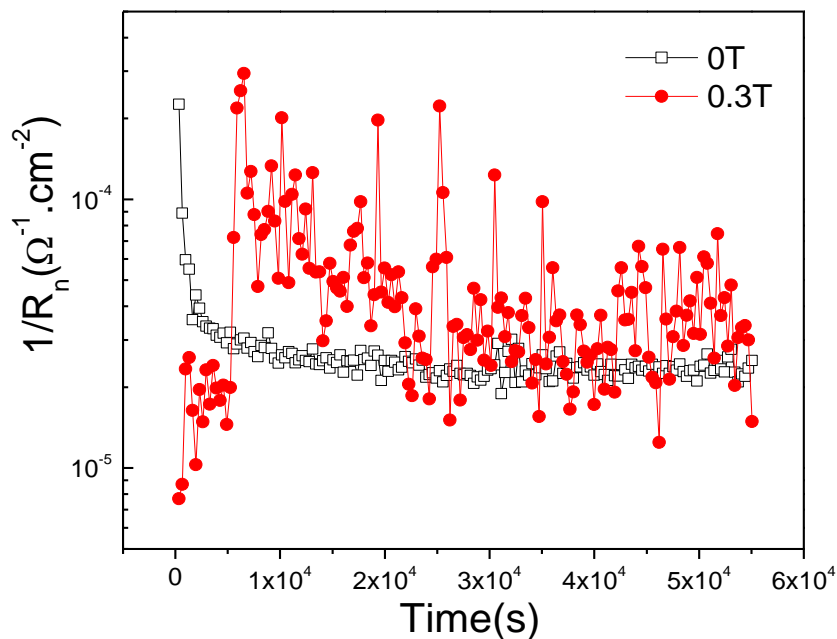


**Figure 6.** S. Wang *et.al.* Submitted to *Int. J. Electrochem. Sci.*

According to the results of the anodic polarization curves, corrosion morphologies and EN measurements, it implied that MF affected the corrosion susceptibility in dual ways during the whole immersion period. The corrosion of pure magnesium in the presence of MF could be divided into two stages, passivation stage and pitting corrosion stage.

5.2 The magnetic field effect on passivation stage of pure magnesium

According to elementary physics, in the presence of the MF, any charged particles will be affected by the Lorentz force,  $F$ ,

$$F = q(v \times B) \tag{8}$$

where  $q$  (coulombs) is the charge on the species moving at velocity  $v$ (m/s) and  $B$  is the applied intensity of the external MF. And it's clear that  $F$  is always perpendicular to  $v$ . Thus an external MF has the ability to alter the rate of molecular transport of electrochemical species which is called the magnetohydrodynamics (MHD) phenomenon [1-16]. The MHD flow in electrochemical systems is conveniently described by the force per unit volume acting on the solution,  $F_{MHD}$  (N/m<sup>3</sup>),

$$F_{MHD} = J \times B \tag{9}$$

where  $J$  is the local flux of ions (C.cm<sup>-2</sup>.s<sup>-1</sup>).

When MF is parallel to the working electrode surface, it will exert a Lorentz force and thus superimpose a MHD velocity ( $V_{mag}$ ) by  $F_{MHD}$  on any charged particle moving in the interfacial diffusion layer which is shown in Fig. 7.  $V_{mag}$  is perpendicular to the MF direction and parallel to the electrode surface. The total velocity ( $V_T$ ) of a charged particle in the presence of MF can be expressed as the vector sum:

$$V_T = V_{mag} + V_{df} \tag{10}$$

where  $V_{df}$  is the velocity of the charged particle due to the concentration gradient.

At first glance, the  $V_{mag}$  was perpendicular with  $V_{df}$ , it seemed that  $V_{mag}$  had no influence on the  $V_{df}$ . However, according to Eq.(10), the presence of MF indicated  $V_T > V_{df}$ . The increasing total velocity implied that a convective flow at the electrode/solution interface was produced by the magnetic field, which leads to the thinning of the interfacial diffusion layer.

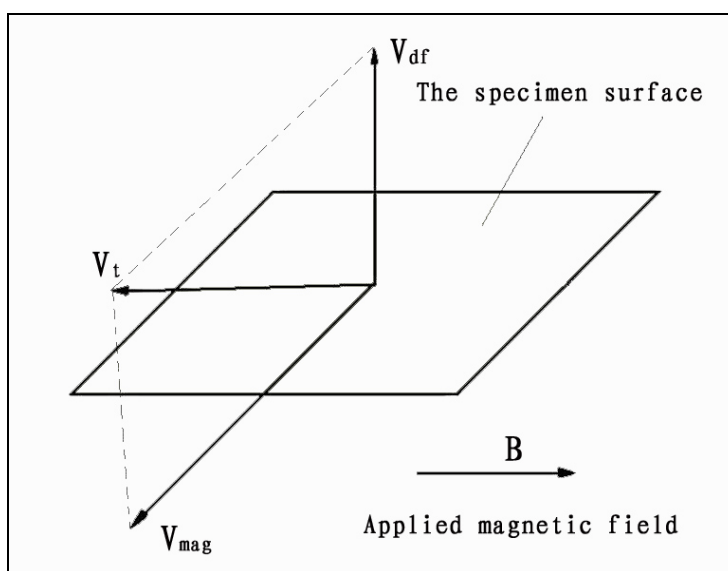
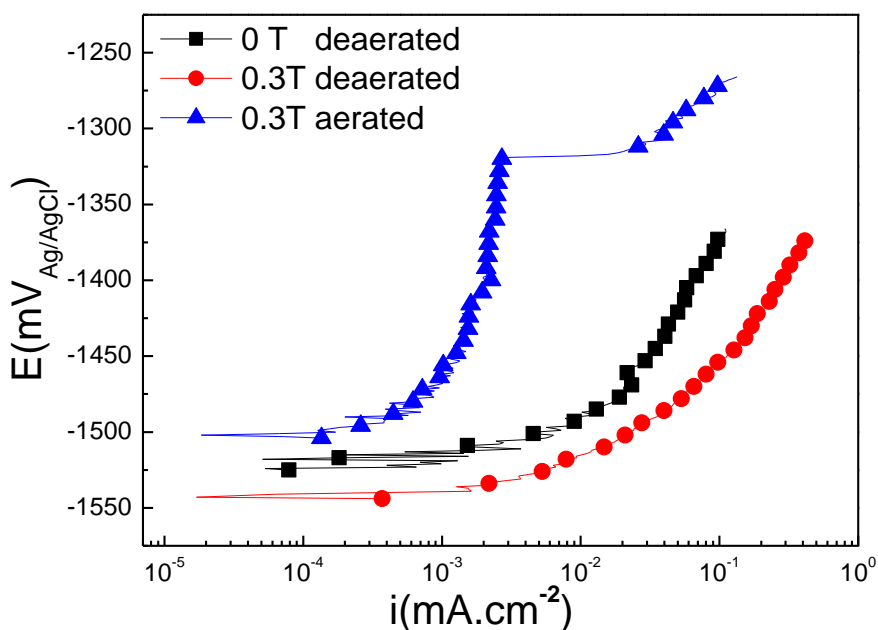


Figure 7. S. Wang et.al. Submitted to Int. J. Electrochem. Sci.

The above review indicates that MF will affect corrosion process from two aspects: first, the mass transfer rate of the polar species, such as  $Mg^+$  and  $Mg^{2+}$ , was increased due to the forced convection of Lorentz force, which suggested that the concentration of  $Mg^+$  and  $Mg^{2+}$  at electrode/solution interface decreased [20]. Hence the anodic dissolution rate of the magnesium would increase in the presence of a magnetic field. Second, the oxygen molecules are neutral and impossible to induce Lorentz force in the presence of MF. However, the forced convection flow produced by the polar species in the presence of MF decreased the thickness of diffusion layer on the electrode/solution interface. According to Fick’s law, the decrease of the diffusion layer thickness indicated the acceleration of the mass transfer process. In the other word, in the presence of MF, the concentration of oxygen at the electrode/solution in the aerated electrolyte would be more sufficient than that in the absence of MF.

Some researches revealed that the oxide film formed on the pure magnesium surface had a better corrosion resistance in the aerated solution than that in the deaerated solution [40, 41]. Therefore, it could be expected that a more perfect surface film formed on magnesium surface and the corrosion resistance was improved, which might be the reason why the magnesium exhibited passive behavior in the beginning of the immersion. If the above discussion was reasonable, once the electrolyte was deaerated, the oxygen environment in the electrolyte should be similar in both absence and presence of MF. Passivation effect of oxygen on the corrosion resistance of magnesium would be minimized to a neglectable extent, so, the anodic dissolution rate of magnesium should be increased by MF.



**Figure 8.** S. Wang *et.al.* Submitted to *Int. J. Electrochem. Sci.*

To confirm this assumption, the anodic polarization curves in the deaerated condition with MF were measured in comparison with that in the aerated condition (Fig. 8). It demonstrated that the polarization curve in the deaerated solution was distinctly different from that in the aerated solution. Firstly, the magnesium in the presence of MF exhibited anodic dissolution behavior instead of passive behavior in the deaerated solution. Secondly, the magnesium in the presence of MF showed a lower corrosion resistance than in the absence of MF. The results of Fig.8 confirmed that our assumption was reasonable. In other word, MF increased the oxygen transportation rate, which led to the passivation of magnesium in the beginning of the immersion.

5.3 The magnetic field effect on pitting corrosion stage of pure magnesium

As the immersion time increased, Cl<sup>-</sup> induced the nucleation randomly occurred. After pitting initiation, the pit was assumed to grow at a certain rate. During the pitting corrosion stage, the susceptibility to pit corrosion was determined to two aspect factors: pitting initiation and pit growth [33, 42, 43]. Pitting initiation determines how the pit forms while pit growth determines whether the pit becomes stable.

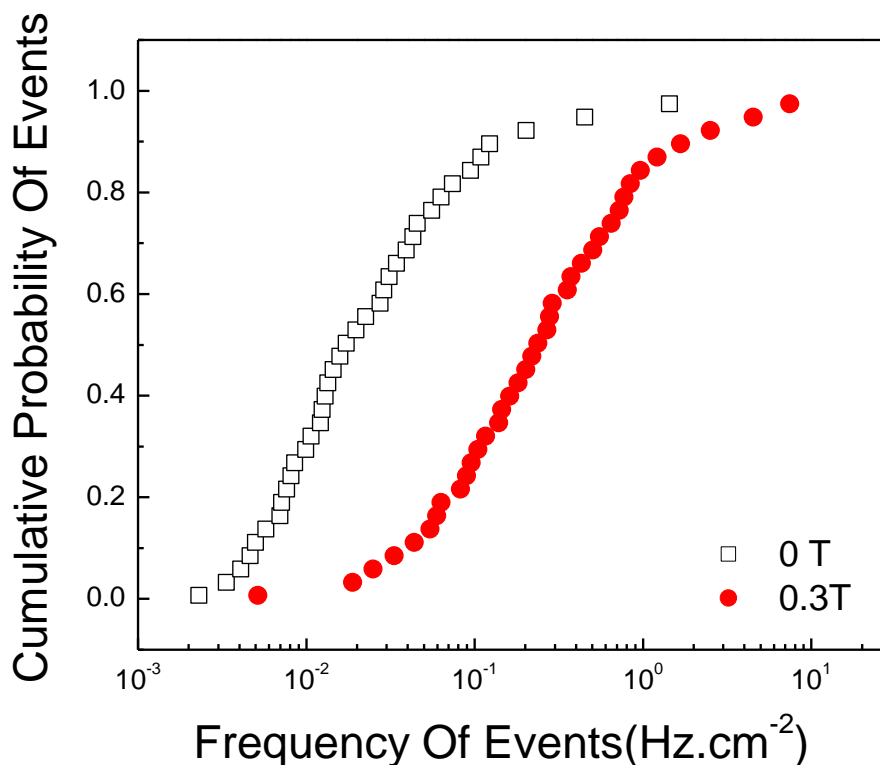


Figure 9. S. Wang et.al. Submitted to Int. J. Electrochem. Sci.

High pitting initiation rate leads to metastable pits spreading all over the specimen surface and high pitting growth rate makes it easy for the pit to grow larger. So a metastable pit which has exceeded a given volume will result in a stable pit.

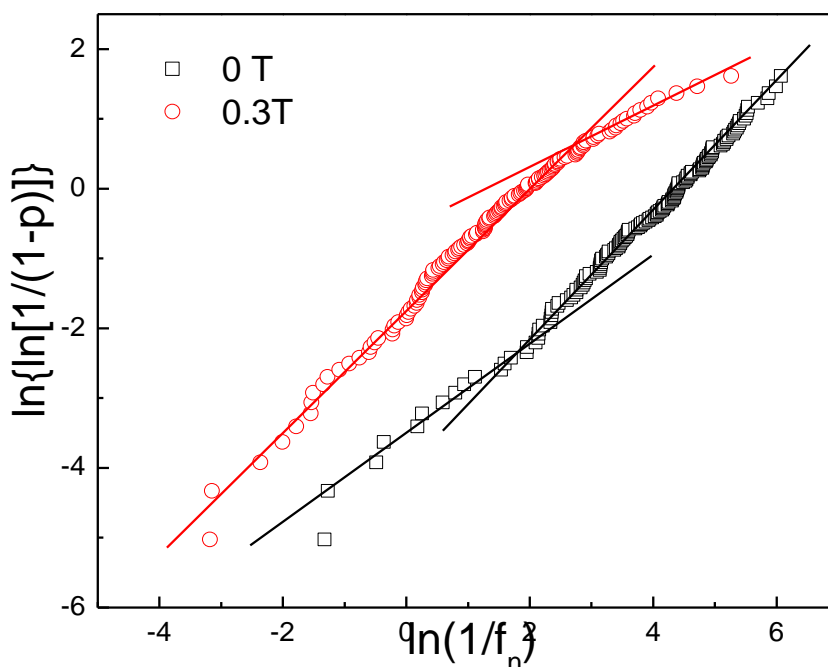
5.3.1 The magnetic field effect on pitting initiation rate of pure magnesium

Fig. 9 presents the cumulative probability plots for  $f_n$  of pure magnesium in the absence and presence of MF, and the parameters needed for the calculation of  $f_n$  were shown in Table 1.

**Table 1.** The fitted electrochemical parameter for the polarization curve of pure magnesium in the absence and presence of magnetic field.

Magnetic intensity (T)	$\beta_a$ (V/decade)	$\beta_c$ (V/decade)	B (V/decade)
0	0.090	0.431	0.209
0.3	0.383	0.407	0.460

It was found that the distribution of  $f_n$  ranged several decades of frequency, indicating that  $f_n$  has a stochastic nature. It was revealed that  $f_n$  provided a relatively good discrimination of pitting corrosion and the distribution of  $f_n$  shifted to a lower frequency region as the corrosion type changed from uniform corrosion to pitting corrosion from the shot-noise theory [44, 45]. The distribution of  $f_n$  was shifted to a higher frequency by MF which implied that corrosion rate of pure magnesium was increased. The shot-noise theory can not provide further information on pitting initiation and pitting growth. In this regard, it is worthwhile to note that there are some research works [46-51] that were devoted to the study on the stochastic analysis of nonhomogeneous Poisson process using Weibull distribution.



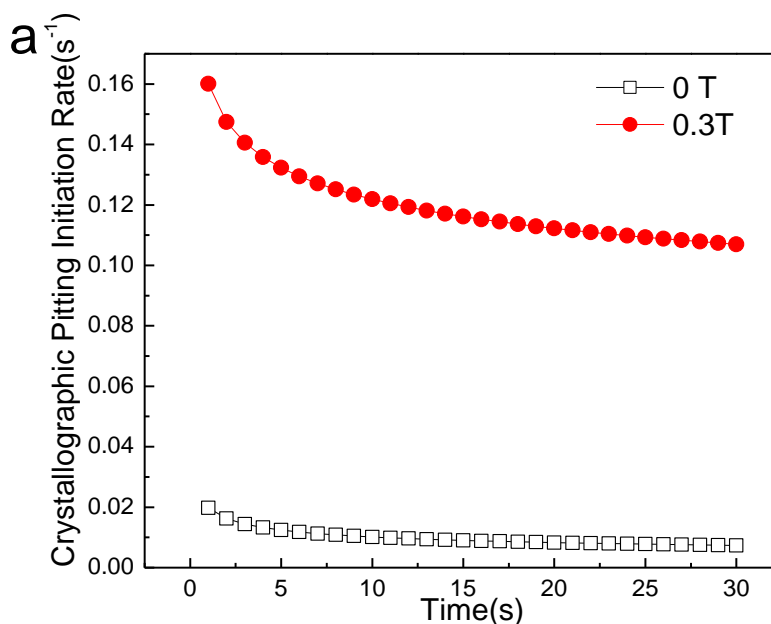
**Figure 10.** S. Wang *et.al.* Submitted to *Int. J. Electrochem. Sci.*

The Weibull probability plots for pure magnesium in the absence and presence of MF was shown in Fig. 10. Two satisfactory straight lines appeared on the plot, which indicated that two failure modes existed, depending upon  $1/f_n$ .

For hexagonal closed packed (hcp) metals, dissolution process has a crystallographic dependence, which means dissolution will first take place in some particular crystallographic orientation (different metals have different crystallographic orientation) [35-37], so crystallographic pitting is considered to be a relatively faster process than pitting corrosion. Therefore, the slopes in the relatively shorter  $1/f_n$  region were associated with dominant crystallographic corrosion. On the other hand, the slopes in the relatively longer  $1/f_n$  region are responsible for dominant pitting corrosion. From Fig. 10, the values of the shape parameter  $m$  and scale parameter  $n$  for pitting corrosion of pure magnesium were determined, which are listed in Table 2.

**Table 2.** Weibull distribution parameters of pure magnesium in the absence and presence of magnetic field

Magnetic intensity (T)	Crystallographic pitting		Pitting corrosion	
	Shape parameters	Location parameters	Shape parameters	Location parameters
	$m$	$n$	$m$	$n$
0	0.709	35.791	0.898	51.403
0.3	0.881	5.505	0.455	1.914



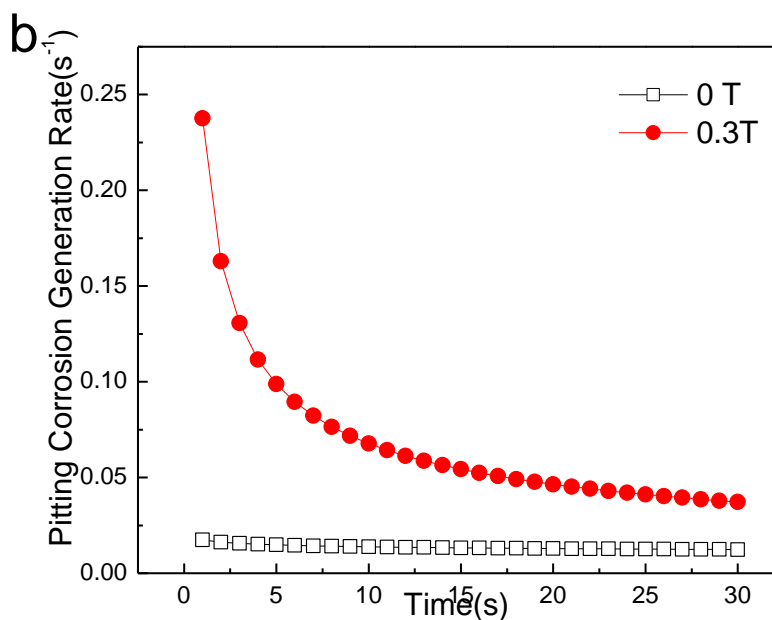
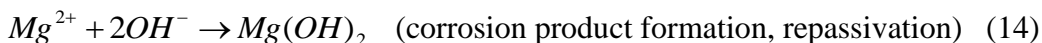


Figure 11. S. Wang et.al. Submitted to Int. J. Electrochem. Sci.

Based upon the concept of conditional probability, in the next unit time, the pitting initiation rate was determined by Eq. (5) using the parameters  $m$  and  $n$  in Table 2. Fig. 11 showed the pitting initiation rate of crystallographic corrosion and pitting corrosion, respectively, both of which indicated that pitting initiation rate was accelerated by MF.

The pitting initiation process of pure magnesium consists of two parallel processes: metastable pitting initiation process and pitting repassivation process. The electrode reactions of pitting embryo process could be stated as [52]:



In the presence of MF, the diffusion rate of  $Mg^+$  and  $Mg^{2+}$  would be accelerated by MHD flow, for the sake of which the  $Mg^+$  and  $Mg^{2+}$  concentration at electrode/solution interface was lower than that in the absence of MF. It indicated that reactions (11) and (12) were increased. Meanwhile, the concentration of the metal ions at electrode/solution interface was decreased due to MHD; so the repassivation rate was decreased by MF (reaction 14).

Taking into consideration of the two factors that the metastable pitting initiation process was accelerated and pitting repassivation process was decelerated, the pitting initiation rate was increased by MF.

5.3.2 The magnetic field effect on pitting growth rate of pure magnesium

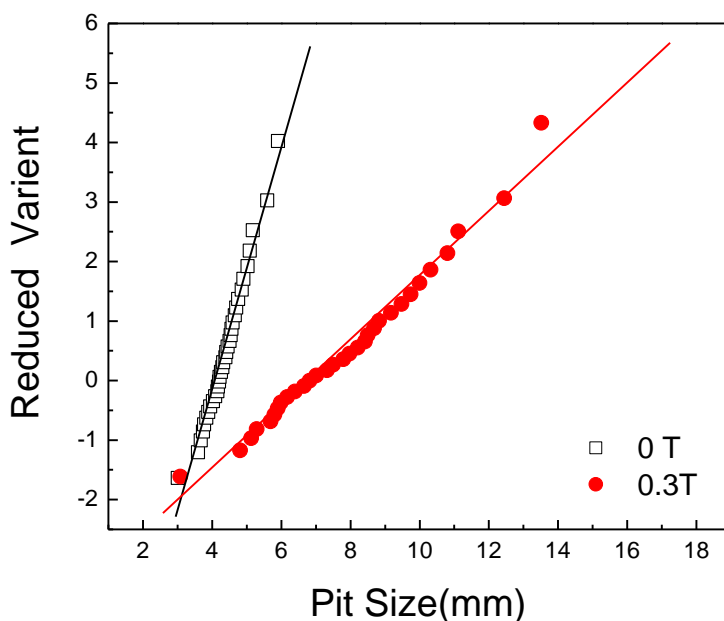


Figure 12. S. Wang et.al. Submitted to Int. J. Electrochem. Sci.

The integration of current transient with time could be used to determine the charge passed for each current transient spike. This charge is the result of the formation of a pit cavity and can be related to the physical volume of the pit by using Faraday’s equation, Eq. (15), which was based on the correlation between optical pit size and anodic current transient charge [53]. If the pits are assumed to be hemispherical the pit radius/depth can be calculated, using Eq. (16):

$$\text{Volume (cm}^3\text{)} = \frac{\text{Charge passed} \times \text{molecular mass}}{\text{Faraday constant} \times n \times \text{density}} \tag{15}$$

$$\text{Pit radius } (\mu\text{m}) = \left( \sqrt[3]{\frac{3 \times \text{volume}(\text{cm}^3)}{2\pi}} \right) \times 10000 \tag{16}$$

The largest pit sizes within each of the EN segments and the values were subjected to extreme value statistics analysis. The Gumbel distribution of pit sizes for pure magnesium in the absence and presence of MF was demonstrated in Fig. 12. Both plots showed only one satisfactory linear region which conformed that the experimental data did in fact fit the Gumbel distribution. The values of  $\alpha$  and  $\mu$  are the scale and location parameters for the distribution of the largest pits respectively which are shown in Table 3.

**Table 3.** Gumbel distribution parameters for pure magnesium in the absence and presence of magnetic field

Magnetic intensity (T)	Scale parameters $\alpha$	Location parameters $\mu$ ( $\mu\text{m}$ )
0	0.459	4.155
0.3	1.865	6.872

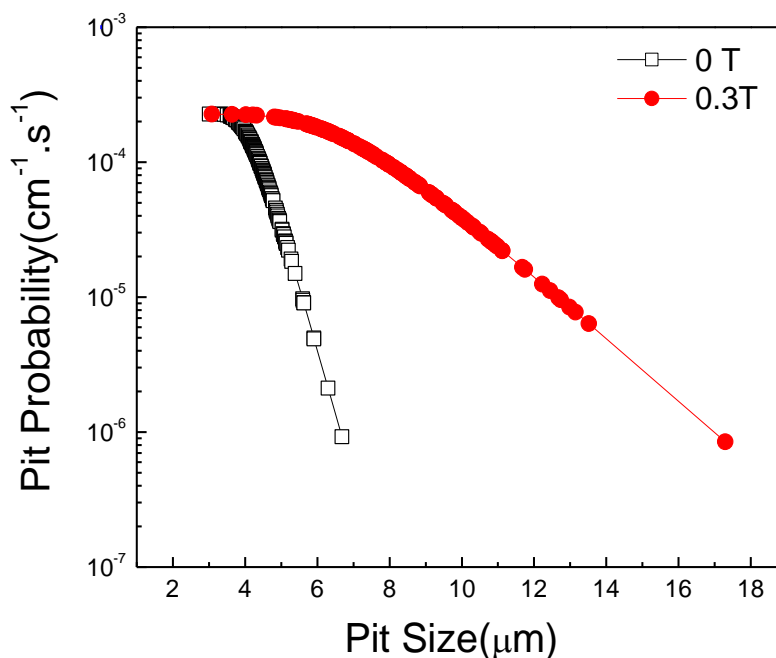


**Figure 13.** S. Wang et.al. Submitted to *Int. J. Electrochem. Sci.*

With Eq. (7) the probability for a given pit radius could be calculated, which were shown in Fig. 13. Since the probability was calculated with the dimensions of time and area, the probabilities can be converted into an expected time for pit cavity with a particular radius to occur by taking the reciprocal of the probability, i.e. calculating the time it takes for the cumulation of the probabilities to equal unity. For example, a pit with a radius of  $6\mu\text{m}$  will occur on the surface of pure magnesium in the absence of MF after 56.40h, while in the presence of MF the occurrence of a pit with the same size

will only take 1.53h. The results indicated that the presence of MF will keep the pitting growth rate at a higher level than that in the absence of MF.

## 6. CONCLUSION

The presence of magnetic field increased the mass transfer rate of the electrode/solution interface produce and the oxygen transportation rate in the electrolyte, which evoked the corrosion susceptibility of pure magnesium in the presence of magnetic field exhibited two distinguishing stage: passivation stage and pitting corrosion stage.

In the passivation stage, magnesium in the presence of magnetic field showed a passive behavior, which indicated that the oxygen transportation played a dominating role in the corrosion of magnesium and a more perfect film formed on magnesium surface. This was confirmed by the deaerated experiment results. During this stage, the corrosion susceptibility of pure magnesium was decreased by magnetic field.

In pitting corrosion stage, the corrosion behavior of pure magnesium turned out to be active dissolution, and serious crystallographic and pitting corrosion began to appear in the presence of magnetic field. The existence of magnetic field increased both the pitting initiation rate and pitting growth rate. In the presence of magnetic field, the pitting initiation process had a higher frequency and initiation rate, which indicated that the crystallographic and pitting corrosion of pure magnesium was increased. With the pitting growth rate increased, the pit had a great probability to grow up and finally developed into a larger pit cavity.

According to all the experiment results, it could be concluded that magnetic field could restrain the corrosion of pure magnesium at the beginning of the immersion and accelerate the corrosion after that. However, taking into account of the whole process of corrosion, the susceptibility of pure magnesium was significantly increased.

## ACKNOWLEDGEMENT

The authors wish to acknowledge the financial support of the National Natural Science Foundation of China (No. 5153000271).

## References

1. A. Rousan, N. Al-Rawashdeh, *Corros. Eng. Sci. Tech.*, 41 (2006) 235.
2. F. Rhen, G. Hinds, J. Coey, *Electrochem. Commun.*, 6 (2004) 413.
3. Y. Tang, A. Davenport, *J. Electrochem. Soc.*, 154 (2007) C362.
4. F. Rhen, D. Fernandez, G. Hinds, J. Coey, *J. Electrochem. Soc.*, 153 (2006) J1.
5. Z. Lu, D. Huang, W. Yang, *J. Congleton, Corros. Sci.*, 45 (2003) 2233.
6. Z. Lu, D. Huang, W. Yang, *Corros. Sci.*, 47 (2005) 1471.
7. Z. Lu, C. Huang, D. Huang, W. Yang, *Corros. Sci.* 48 (2006) 3049.
8. Z. Lu, W. Yang, *Corros. Sci.*, 50 (2008) 510.
9. T. Fahidy *J. Appl. Electrochem.*, 13 (1983) 553-563.
10. O. Aaboubi, J.P. Chopart, J. Douglade, A. Olivier, C. Gabrielli, B. Tribollet, *J. Electrochem. Soc.*, 137 (1990) 1796.
11. R. Tacke, L. Janssen, *J. Appl. Electrochem.*, 25 (1995) 1.

12. R. Sueptitz, K. Tschulik, M. Uhlemann, L. Schultz and A. Gebert, *Electrochim. Acta*, 56 (2011) 5866
13. M. C. Gázquez, T. Hernández, F. Muktepavela, E. Platacis and A. Shishko, *J. Nuclear Mater.*, 465 (2015) 633
14. K. Boumhara, M. Tabyaoui, C. Jama, F. Bentiss, *J. Indust. Eng. Chem.*, 29 (2015) 146
15. K. Shinohara, K. Hashimoto, R. Aogaki, *Chem. Lett.* 31 (2002) 738.
16. K. Shinohara, R. Aogaki, *Electrochem.* 67 (1999) 126.
17. A. Chiba, K. Kawazu, O. Nakano, T. Tamura, S. Yoshihara, E. Sato, *Corros. Sci.* 36 (1994) 539.
18. A. Ručinskienė, G. Bikulčius, L. Gudavičiūtė, E. Juzeliūnas, *Electrochem. Commun.* 4 (2002) 86.
19. P. Linhardt, G. Ball, E. Schlemmer, *Corros. Sci.* 47 (2005) 1599.
20. J. Li, T. Zhang, Y. Shao, G. Meng and F. Wang, *Mater. Corros.*, 61(2010) 306.
21. X. Liu, T. Zhang, Y. Shao, G. Meng, F. Wang, *Corros. Sci.*, 52 (2010) 892.
22. G. Song, D. StJohn, *Corros. Sci.*, 46 (2004) 1381.
23. R. Cottis, *Corros.*, 57 (2001) 265.
24. H. Al-Mazeedi, R. Cottis, *Electrochim. Acta*, 49 (2004) 2787.
25. J. Sanchez-Amaya, R. Cottis, F. Botana, *Corros. Sci.*, 47 (2005) 3280.
26. A. Valor, F. Caleyó, L. Alfonso, D. Rivas, J. Hallen, *Corros. Sci.*, 49 (2007) 559.
27. E. Lewis, Introduction to reliability engineering, John Wiley and Sons, New York, 1987.
28. S. Pyun, E. Lee, G. Han, *Thin Solid Films.*, 239 (1994) 74.
29. J. Park, S. Pyun, *Corros. Sci.*, 46 (2004) 285.
30. E.J. Gumbel, Statistics of Extremes, Columbia University Press, NY, 1957.
31. A. Trueman, *Corros. Sci.*, 47 (2005) 2240.
32. A. Turnbull, *Brit. Corros. J.*, 28 (1993) 297.
33. G. Engelhardt, D. Macdonald, *Corros. Sci.*, 46 (2004) 2755.
34. A. Tahara, T. Shinohara, *Corros. Sci.*, 47 (2005) 2589.
35. C. McCall, M. Hill, R. Lillard, *Corros. Eng. Sci. Tech.*, 40 (2005) 337.
36. P. Schmutz, V. Guillaumin, R. Lillard, J. Lillard, G. Frankela, *J. Electrochem. Soc.*, 150 (2003) B99.
37. R. Lillard, G. Wang, and M. Baskes, *J. Electrochem. Soc.*, 153 (2006) B358.
38. Y. Song, D. Shan, E. Han, *Corros. Sci.*, 52 (2010) 1830.
39. B. Ramezanzadeh, S. Arman, M. Mehdipour, B. Markhali, *Appl. Surf. Sci.*, 289 (2014) 129
40. N. Upadhyay, M. Pujar, C. Das, C. Mallika, U. Mudal, *Corros.*, 70 (2014) 781.
41. G. Baril, N. Pebere, *Corros. Sci.*, 43 (2001) 471.
42. T. Zhang, C. Chen, Y. Shao, G. Meng, F. Wang, X. Li, C. Dong, *Electrochim. Acta*, 53 (2008) 7921.
43. A. Valor, F. Caleyó, L. Alfonso, D. Rivas, J. Hallen, *Corros. Sci.*, 49 (2007) 559.
44. H. Al-Mazeedi, R. Cottis, *Electrochim. Acta*, 49 (2004) 2787.
45. J. Sanchez-Amaya, R. Cottis, F. Botana, *Corros. Sci.*, 47 (2005) 3280.
46. K. Na, S. Pyun, *Electrochim. Acta*, 52 (2007) 4363.
47. K. Na, S. Pyun, H. Kim, *Corros. Sci.*, 49 (2007) 220.
48. K. Na, S. Pyun, *Corros. Sci.* 49 (2007) 2663.
49. K. Na, S. Pyun, *Corros. Sci.*, 50 (2008) 248.
50. K. Na, S. Pyun, *J. Electrochem. Soc.*, 154 (2007) C355.
51. K. Na, S. Pyun, *J. Electroanal. Chem.*, 596 (2006) 7.
52. G. Song, A. Atrens, *Adv. Eng. Mater.*, 12 (2003) 837.
53. S. Pride, J. Scully, J. Hudson, *J. Electrochem. Soc.*, 141 (1994) 3028.